Journal of Materials Chemistry A

ROYAL SOCIETY OF CHEMISTRY

PAPER

View Article Online
View Journal | View Issue

Cite this: *J. Mater. Chem. A*, 2020, **8**, 13049

Volatilizable and cost-effective quinone-based solid additives for improving photovoltaic performance and morphological stability in non-fullerene polymer solar cells†

Youdi Zhang,‡[ab] Yongjoon Cho,‡[a] Jungho Lee,[a] Jiyeon Oh,[a] So-Huei Kang,[a] Sang Myeon Lee,[a] Byongkyu Lee,[a] Lian Zhong,[a] Bin Huang,[a] Seungjin Lee,[c] Jin-Woo Lee,[c] Bumjoon J. Kim,[c] Yongfang Li[d] and Changduk Yang*[a]

Controlling the morphological stability of non-fullerene polymer solar cells (NF-PSCs) is a critical process for improving photovoltaic performances. In many systems, liquid additives have been widely used to produce favorable morphological features; however, liquid additives frequently leave residues after thermal treatment owing to their high boiling points, which has detrimental effects on the reproducibility of NF-PSCs. In this study, commercially available and volatilizable solid additives, 9,10-anthracenedione (BDT-1) and benzo[1,2-*b*:4,5-*b*′]dithiophene-4,8-dione (BDT-2), are selected to coordinate the molecular arrangement to enhance absorption intensity, charge transfer, and molecular crystallinity. Suppressed bimolecular recombination and a favorable balance between the domain size and relative domain purity were observed with the introduction of both solid additives, which improved the photovoltaic parameters of NF-PSCs. PM6:TPT10-based devices with BDT-1 and BDT-2 additives achieved the best power conversion efficiencies (PCEs) of 16.26% and 15.18%, respectively, which were better than the 13.55% achieved with a 1,8-diiodooctane (DIO) additive. Other NF-PSC systems of PBDB-T:TPT10 and PTQ10:TPT10 blends also showed that the photovoltaic performance with the solid additives is superior to that with liquid additives. These results imply that the use of solid additives is a promising strategy to improve the PCEs of NF-PSCs.

Received 13th May 2020
Accepted 11th June 2020

DOI: 10.1039/d0ta04941g

rsc.li/materials-a

Introduction

Polymer solar cells (PSCs) have reached a stage of rapid development,[1–21] and some new device structures, such as flexible[22–25] and semitransparent[26,27] PSC devices, and new device-processing methods, such as roll-to-roll,[28] screen printing,[29] inkjet printing,[30] *etc.* are moving toward market applications. The main reason for studying PSCs is their unique advantages such as low-cost solution processing, flexibility, and light weight. In recent years, the power conversion efficiencies (PCEs) of PSCs have rapidly improved owing to the development of novel donor and acceptor materials, especially non-fullerene small molecule acceptors such as Y6,[31] which employs a ladder-type A–DA′D–A structure with a benzothiadiazole (BT) core in its DA′D fused ring central unit. By adopting new polymer donors, morphology optimization strategies, interfacial engineering control, and new device manufacturing methods, the PCEs of PSCs were boosted to over 16% for bulk heterojunction binary PSCs and to over 17% for ternary PSCs.[32–45] In addition, optimized charge generation, transport and collection and reduced carrier recombination lead to a nanostructured fiber morphology of bi-continuous interpenetrating networks resulting in a considerably improved efficiency of PSCs fabricated with a small amount of liquid additives and thermal/vapor annealing to optimize the morphology of the active layer.[46]

In photovoltaic devices, the optimization of the active layer morphology is essential for improving the efficiency of PSCs.[47] To form an ideal nanoscale phase morphology of donor/acceptor dual continuous interpenetrating network structures, several preparation methods have been used to optimize the blend morphology, *i.e.*, the use of small amounts of liquid

[a]*Department of Energy Engineering, School of Energy and Chemical Engineering, Perovtronics Research Center, Low Dimensional Carbon Materials Center, Ulsan National Institute of Science and Technology (UNIST), 50 UNIST-gil, Ulju-gun, Ulsan 44919, Republic of Korea. E-mail: yang@unist.ac.kr*

[b]*College of Chemistry, Nanchang University, 999 Xuefu Avenue, Nanchang 330031, China*

[c]*Department of Chemical and Biomolecular Engineering, Korea Advanced Institute of Science and Technology (KAIST), Daejeon, 34141, Republic of Korea*

[d]*Beijing National Laboratory for Molecular Sciences, CAS Key Laboratory of Organic Solids, Institute of Chemistry, Chinese Academy of Sciences, Beijing 100190, China*

† Electronic supplementary information (ESI) available. See DOI: 10.1039/d0ta04941g

‡ Y. Zhang and Y. Cho contributed equally to this work.

additives,[48] thermal annealing (TA),[49] and solvent vapor annealing.[50] Previously reported outstanding high-boiling-point liquid additives, 1,8-octanedithiol (ODT), 1,8-diiodooctane (DIO), nitrobenzene (NB), *N*-methylpyrrolidone (NMP), 1-chloronaphthalene (1-CN), diphenyl ether (DPE), 1-phenylnaphthalene (PN), 1,2,3,4-tetrahydronaphthalene (THN), and 1-methyl-naphthalene, have been used to modulate a favorable micro-phase morphology of D/A photovoltaic blends.[51–56] This approach facilitates better phase separation, domain size, and phase purity and, consequently, enhances the intermolecular π–π stacking to balance the charge transport channel for the PSCs.[57] Currently, the micro-nanomorphology of NF-based blends is successfully prepared by following these empirical strategies to produce highly efficient PSCs. The particular intermolecular interaction features of blends and the manufacturing method are considered and explored to optimize the blend morphology. Achieving good device stability and reproducibility is crucial for the further development of PSCs. Nevertheless, to enhance the efficiency of PSCs, using the liquid additive is not a reliable processing method. The reproducibility of the device performance is considerably undermined by adopting these liquid additives because the PCE of PSCs is more sensitive to the liquid additive content and molecular structure, and the residual high-boiling-point additive in the active layer considerably affects or delays the drying procedure, which results in a dissatisfactory geomorphological feature. It is known that a small amount of residual additive accelerates photo-oxidative deterioration and considerably degrades the lifetime of the device.[58] The removal of these liquid additives is relatively difficult. Several controlled methods have been adopted that involve high-vacuum equipment, high-temperature TA, and washing the blend with an interface layer-modifying solvent. However, these strategies cannot eliminate the above-mentioned problems caused by these liquid additives. Thus, it is essential to develop a new method. Recently, the use of solid additives (SAs), as a simple and promising modification strategy, has shown several excellent advantages.[32,40,41,59,60] Specifically, (1) SAs not only induce redshifted absorption, but also increase the absorption coefficient of a blend film, which is conducive to obtaining a higher short-circuit current density (J_{SC}) value; (2) SAs can boost the intermolecular π–π stacking and promote the charge carrier mobility, which is beneficial for achieving high PCEs of PSCs; (3) importantly, the use of volatilizable SAs allows fabricating photovoltaic devices that exhibit better long-term stability and reproducibility. These advantages demonstrate a promising strategy to develop new SAs to improve the NF-PSC device properties.

In this study, the use of commercial and volatilizable SAs increased the intermolecular π–π interaction of blends in NF-PSCs. The SAs, 9,10-anthracenedione (BDT-1) and benzo[1,2-*b*:4,5-*b*′]dithiophene-4,8-dione (BDT-2), were selected to optimize the blend morphology, which further improved the PCEs of NF-PSCs. The absorption spectra demonstrate that the SA films, the BDT-1 and BDT-2 films, underwent TA at 140 °C and easily evaporated from the glass substrate. To show that this is an effective strategy, we used three popular conjugated polymer donors (PM6,[61] PBDB-T,[62] and PTQ10 (ref. 46)), a Y6-derivative acceptor TPT10 (ref. 38) with monobrominated end groups, and BDT-1 as the SA to fabricate PSC devices and optimized the morphology of the photovoltaic active layer. The optimized PSC based on PM6:TPT10 showed a high PCE value up to 16.26%, which is higher than that of the device using 1,8-diiodooctane (DIO) as a liquid additive. More importantly, SAs not only increased the absorption intensity, formed an optimized micro-nanoscale blend morphology, improved the charge carrier mobilities, considerably suppressed bimolecular recombination, and accommodated the compatibility of the donor and acceptor, but also led to good thermal and photo-induced stability and reproducibility of the photovoltaic performance of the devices. The results demonstrate that using a SA is a positive and effective method for producing highly efficient PSCs.

Results and discussion

Fig. 1a shows the chemical structure of the polymer donors PM6, PBDB-T, and PTQ10, acceptor TPT10, and two SAs BDT-1 and BDT-2. Two SAs with similar chemical structures were selected for the systematic investigation of the volatilization effect. To confirm the volatility of SAs, neat BDT-1 and BDT-2 solutions in chloroform were spin-coated on a silicon substrate. After the TA treatment of the films at 140 °C for 10 min, we observed the smooth surface of the silicon substrate with the naked eye, which implied that SAs were easily removed by the TA treatment (Fig. 1b). The intensity of the absorption spectra of the SA films was reduced to close to zero after the TA treatment (Fig. S1, in the ESI†), which further confirmed the volatility of the SAs. Interestingly, the volatility seems greater for BDT-1 despite its higher molecular weight than that of BDT-2. The lowest unoccupied molecular orbital (LUMO) energy levels and the highest occupied molecular orbital (HOMO) energy levels of the previously reported polymer donors PM6, PBDB-T, and PTQ10 and acceptor TPT10 were −3.61/−5.50, −2.92/−5.33, −2.98/−5.54, and −3.99/−5.52 eV, respectively (Fig. 1c). Clearly, the PM6:TPT10 and PTQ10:TPT10 blends tend to achieve a high open-circuit voltage (V_{OC}) value. In addition, Fig. 2a shows the absorption spectra of the polymer donors PM6, PBDB-T, and PTQ10 and acceptor TPT10, which demonstrates that the absorption range of the conjugated polymer donors is complementary to that of the acceptor molecule. To explore the effect of SAs on the absorption intensity of the blends, Fig. 2b–d show the absorption spectra of PM6:TPT10, PBDB-T:TPT10, and PTQ10:TPT10 blends with a DIO liquid additive and BDT-1 and BDT-2 SAs, respectively. The absorption spectra of the blend films with BDT-1 and BDT-2 are broader and show a stronger molar extinction coefficient compared to those of the blends with a DIO additive. Of note, the PM6:TPT10 blend with the BDT-1 additive shows the highest absorption coefficient of 8.23×10^4 cm^{-1} among all the blend films. Consequently, SAs considerably increase the redshift, width, and peak strength of the absorption spectra, which is beneficial for obtaining a high J_{SC} value.

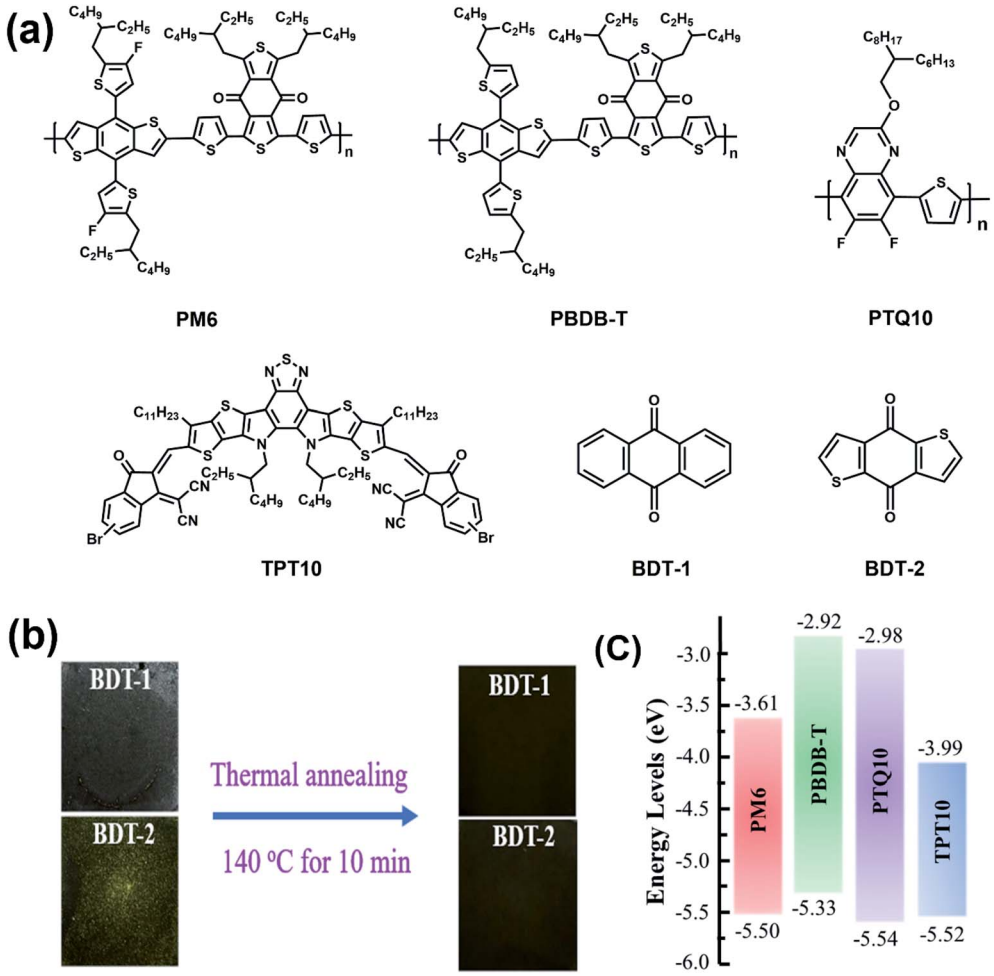

Fig. 1 (a) Chemical structures of the polymer donors PM6, PBDB-T, and PTQ10, acceptor TPT10, and two SAs BDT-1 and BDT-2; (b) photographs of spin-coated films of the two SAs on a Si substrate followed by thermal annealing at 140 °C for 10 min; (c) energy diagrams for the used materials.

To investigate the effect of SAs on the photovoltaic performance, BDT-1 and BDT-2 are employed in PM6:TPT10, PBDB-T:TPT10, and PTQ10:TPT10-based PSCs to optimize photovoltaic efficiencies with a conventional device structure of ITO/PEDOT:PSS/active layer/PDINO/Al, where ITO is indium tin oxide, PEDOT is poly(3,4-ethylenedioxythiophene), PSS is poly(styrene sulfonate), and PDINO is a perylene diimide (PDI) derivative with amino N-oxide terminal substituent cathode interlayers. Fig. 3a and S2† show the current density–voltage (*J*–*V*) plots of the devices with different additives (*i.e.*, DIO, BDT-1, and BDT-2) under the illumination of an AM 1.5G solar simulator at 100 mW cm^{-2}; the relevant photovoltaic parameters are summarized in Table 1 and S1.† First, we applied two SAs, BDT-1 and BDT-2, to a photovoltaic systems based on PM6:TPT10, PBDB-T:TPT10, and PTQ10:TPTP10, and a control system with a liquid additive DIO was also prepared for the same blends. The control device of PM6:TPT10 with a 0.25% DIO additive, which was thermally annealed at 110 °C for 10 min, achieved a PCE of 13.55% with a V_{OC} of 0.877 V, a J_{SC} of 22.40 mA cm^{-2}, and a fill factor (FF) of 68.60%. A different amount of BDT-1 and BDT-2 than of DIO was used to optimize the same photovoltaic active layer system; we determined that the PM6:TPT10 device with the BDT-1 additive with TA at 140 °C for 10 min achieved the highest PCE of 16.26% with a V_{OC} of 0.899 V, J_{SC} of 24.80 mA cm^{-2}, and FF of 73.00% when the weight ratio of the SA to the total system was 16 wt%, which is superior to that of the device (15.18%) with the BDT-2 additive. In addition, the SAs BDT-1 and BDT-2 were applied to other photovoltaic systems and also showed the same trend. For the PBDB-T:TPT10-based device, the PSC with a 16 wt% BDT-1 additive obtained an optimized PCE of 13.41% with a V_{OC} of 0.783 V, J_{SC} of 24.90 mA cm^{-2}, and FF of 68.80%, which is higher than the 12.60% with 16 wt% BDT-2 and 10.86% with a 0.25% DIO additive. The PTQ10:TPTP10-based device with a 16 wt% BDT-1 additive produced the best photovoltaic performance with a PCE of up to 13.14%. Other device data with SAs of different weight ratios are listed in Table S1.† The SA BDT-1 shows excellent properties in promoting the photovoltaic performance of NF-PSCs by enhancing all photovoltaic parameters (V_{OC}, J_{SC}, and FF) at the same time. These results adequately demonstrate that the simple application of commercial and volatilizable SAs can be

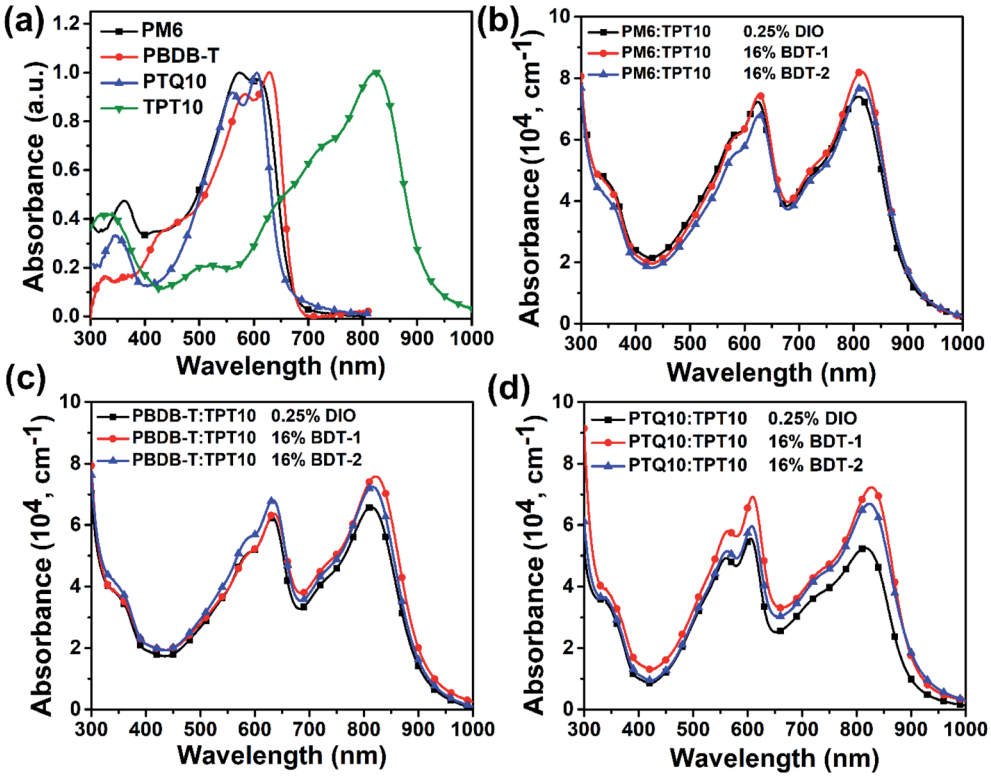

Fig. 2 The absorption spectra of the polymer donors PM6, PBDB-T, and PTQ10 and acceptor TPT10 films (a); the absorption intensity of PM6:TPT10 (b), PBDB-T:TPT10 (c), and PTQ10:TPT10 (d) blends (1 : 1.2, w/w) with 0.25% DIO, 16 wt% BDT-1, and 16 wt% BDT-2 additives after thermal annealing, respectively.

an effective and convenient strategy for increasing the PCE of NF-PSCs.

Fig. 3b and S2† show the external quantum efficiency (EQE) plots, in which the control device, which is based on PM6:TPT10 with a 0.25% DIO liquid additive, produced an integrated current of 21.23 mA cm^{-2}. Compared to the control device, the BDT-1 and BDT-2-treated devices showed strong and red-shifted photoresponses, which is consistent with the absorption spectra of the blends, and produced reliable integrated current densities of 23.91 mA cm^{-2} and 23.71 mA cm^{-2}, respectively. By investigating PBDB-T:TPT10 and PTQ10:TPT10-based devices, a performance improvement is observed for the SA-treated devices similar to that of the PM6:TPT10-based devices. However, the EQE values of the devices based on PBDB-T:TPT10 and PTQ10:TPT10 are lower than those of the PM6:TPT10-based device. Of note, the use of SAs enhances the photoresponse of

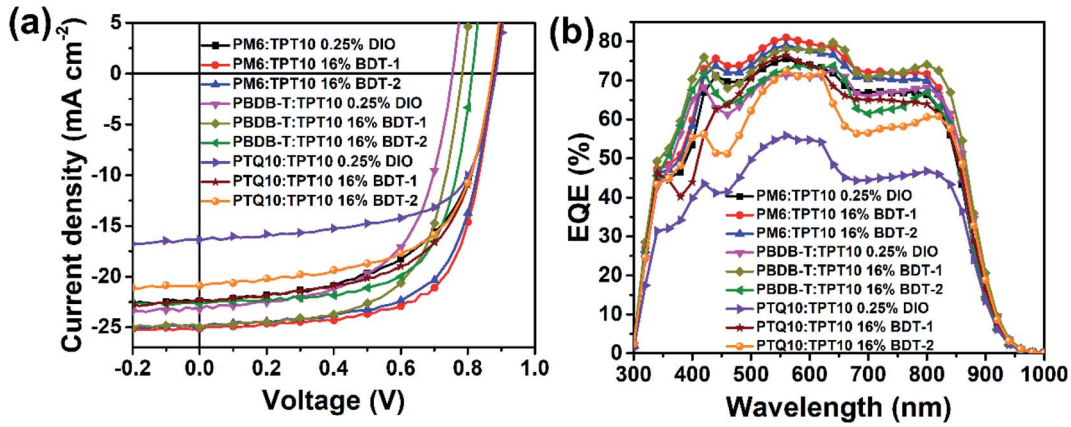

Fig. 3 (a) The *J*–*V* plots of the PM6:TPT10, PBDB-T:TPT10, and PTQ10:TPT10-based PSCs (1 : 1.2, w/w) with 0.25% DIO, 16 wt% BDT-1, and 16 wt% BDT-2 additives after thermal annealing in the blend films under simulated AM 1.5G irradiation (100 mW cm^{-2}); (b) EQE spectra of the corresponding polymer solar cells.

Table 1 The photovoltaic parameters of the optimized PSCs (1 : 1.2, w/w) with 0.25% DIO, 16 wt% BDT-1, and 16 wt% BDT-2 additives after thermal annealing

Blends	Additives	TA	V_{OC} (V)	J_{SC} (mA cm^{-2})	FF (%)	PCE[a] (ave.) (%)
PM6:TPT10	0.25% DIO	110 °C	0.877	22.40 (21.23)[b]	68.60	13.55 (13.21 ± 0.20)
	16 wt% BDT-1	140 °C	0.899	24.80 (23.91)	73.00	16.26 (15.95 ± 0.13)
	16 wt% BDT-2	140 °C	0.877	24.90 (23.73)	69.50	15.18 (15.03 ± 0.11)
PBDB-T:TPT10	0.25% DIO	110 °C	0.754	23.20 (22.03)	62.10	10.86 (10.57 ± 0.21)
	16 wt% BDT-1	140 °C	0.783	24.90 (23.73)	68.80	13.41 (13.20 ± 0.15)
	16 wt% BDT-2	140 °C	0.813	22.70 (21.53)	68.30	12.60 (12.35 ± 0.18)
PTQ10:TPT10	0.25% DIO	70 °C	0.883	16.40 (15.23)	63.80	9.21 (9.05 ± 0.10)
	16 wt% BDT-1	140 °C	0.890	22.30 (21.15)	66.20	13.14 (12.85 ± 0.22)
	16 wt% BDT-2	140 °C	0.873	20.90 (19.73)	66.80	12.37 (12.13 ± 0.16)

[a] Average values in brackets calculated from 20 devices are outlined in parentheses. [b] Values in brackets are calculated from the EQE spectra.

photovoltaic devices in the long-wavelength ranges, compared with the liquid additive. All integrated current densities of the devices obtained from the EQE spectra agreed well with those obtained from the *J–V* measurements.

To obtain a deeper insight into the charge carrier recombination mechanism of the PSCs based on PM6:TPT10, PBDB-T:TPT10, and PTQ10:TPT10, the light intensity-dependent J_{SC} and V_{OC} characteristics were evaluated. The exciton dissociation efficiency ($\eta_{diss} = J_{ph}/J_{sat}$) and charge collection efficiency ($\eta_{coll} = J^{\#}_{ph}/J_{sat}$, where $J^{\#}_{ph}$ is the compensation electric current under maximized power output) were determined from the curves of photocurrent density (J_{ph}) *versus* effective voltage (V_{eff}) at J_{SC} and under maximum power output conditions,[63] as shown in Fig. 4 and S3;† J_{ph} was determined using $J_{ph} = J_L - J_D$, where J_L and J_D are the current densities under illumination of AM 1.5G, 100 mW cm^{-2} and under dark conditions, respectively. $V_{eff} = V_0 - V_{appl}$, where V_0 is the voltage at which $J_{ph} = 0$, and V_{appl} is the applied bias voltage. The saturated photocurrent was observed at V_{eff} = 2–4 V, and the relevant parameters of J_{ph}, $J^{\#}_{ph}$, J_{sat}, η_{diss}, and η_{coll} are outlined in Table S2.† The η_{diss} values were calculated to be 99%, 97%, and 95% for PM6:TPT10, PBDB-T:TPT10, and PTQ10:TPT10 blends with 16 wt% BDT-1 additive under short-circuit conditions, which is higher than those of the devices with 16 wt% BDT-2 additive (η_{diss} of 98, 96, and 94%), respectively. The devices based on PM6:TPT10, PBDB-T:TPT10, and PTQ10:TPT10 with 16 wt% BDT-1 additive showed η_{coll} values of 90, 86, and 81%, which are superior to those of the devices with 16 wt% BDT-2, respectively. It is clear that the η_{diss} and η_{coll} of the devices with SAs surpass those of the blends with a liquid additive. The higher η_{diss} and η_{coll} values of 99% and 90% for the PM6:TPT10 blend with the 16 wt% BDT-1 additive treatment are consistent with the superior photovoltaic performance of the devices compared with those of the control devices with 0.25% DIO solvent additive.

The light intensity (P) dependence of J_{SC} and V_{OC} was also evaluated to determine the non-geminate recombination losses of the devices.[64,65] The relationship between J_{SC} and light intensity follows the relation of $J_{sc} \propto P^S$. The S values of the device based on PM6:TPT10 with 0.25% DIO, 16 wt% BDT-1, and 16 wt% BDT-2 additives were determined to be 0.95, 0.99, and 0.97, respectively, from the log J_{SC}–log P plots in Fig. 4b. The S value of 0.99 (near 1.00) for the device with 16 wt% BDT-1 additive and TA for 10 min shows that bimolecular recombination was inappreciable in the PM6:TPT10-based device, which is lower than that for other devices based on PBDB-T:TPT10 and PTQ10:TPT10; this result indicates that all free carrier charges are separated in the donor/acceptor interfaces and collected at the electrodes. The devices based on PBDB-T:TPT10 and PTQ10:TPT10 exhibited dissatisfactory S values (far from 1.00), as shown in Fig. S3b and S3e.† These results indicate that the PM6:TPT10 device with SAs showed a smaller geminate recombination loss that exceeds those of other devices. The V_{oc}–ln P curves are shown in Fig. 4c; V_{oc} exhibits a light intensity dependence with a slope of 1.13, 1.05, and 1.08 kT per q for the PM6:TPT10-based device with the treatments of

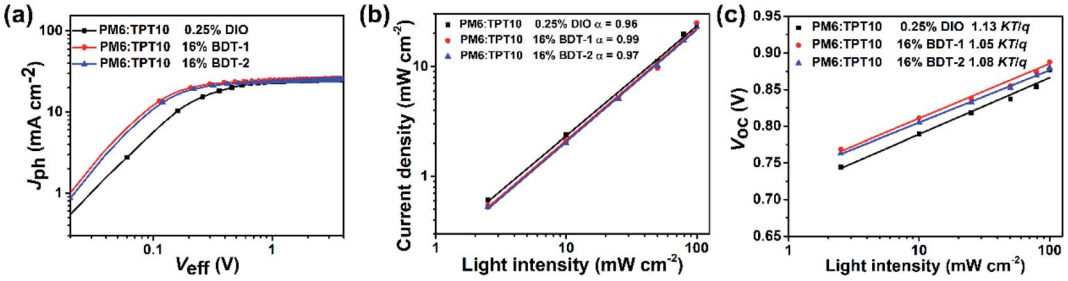

Fig. 4 J_{ph}–V_{eff} (a), J_{SC}–P (b), and V_{OC}–P (c) curves of PM6:TPT10 (1 : 1.2, w/w) based devices with 0.25% DIO, 16 wt% BDT-1, and 16 wt% BDT-2 additives after thermal annealing. The solid lines indicate fitted curves in J_{SC}–P and V_{OC}–P plots.

0.25% DIO, 16 wt% BDT-1, and 16 wt% BDT-2 additives, respectively. Fig. S3c and S3f† show that the slopes for PBDB-T:TPT10 and PTQ10:TPT10 with 0.25% DIO, 16 wt% BDT-1, and 16 wt% BDT-2 additives are larger (more deviated from 1 kT per q) than those of the PM6:TPT10 device. The slopes of all devices with SAs are more close to 1 kT per q compared with those of devices with liquid additives. The results indicate that the optimized PM6:TPT10-based device shows less charge-trapped recombination, which was consistent with the elevated PCE of the NF-PSCs. These data adequately demonstrate that the bimolecular recombination loss and space-charge effect are prohibited under J_{SC} conditions for the devices with a SA treatment.

To evaluate the effect of SA treatments on the photovoltaic properties of the NF-PSCs based on PM6:TPT10, PBDB-T:TPT10, and PTQ10:TPT10 and to investigate why J_{SC} and FF can be simultaneously enhanced in the blend films with BDT-1 or BDT-2, the electron (μ_e) and hole (μ_h) mobilities of the blend films were measured by the space charge limited current (SCLC)[66] method with an electron-only device structure of ITO/ZnO/active layer/PDINO/Al and a hole-only device structure of ITO/PEDOT:PSS/active layer/MoO_3/Au. As shown in Fig. S4 and Table S3,† μ_e and μ_h of blends with SAs are superior to those of the device with a liquid additive, and μ_h values are higher than μ_e values in all devices, which indicates that μ_e is essential for limiting the photovoltaic performance, in particular for J_{SC} and FF. The μ_e of the device based on PM6:TPT10 with BDT-1/TA is 6.78×10^{-4} cm^2 V^{-1} s^{-1}, which is higher than that of the device with BDT-2/TA (5.21×10^{-4} cm^2 V^{-1} s^{-1}) and DIO/TA (4.74×10^{-4} cm^2 V^{-1} s^{-1}), while the μ_h of the device with DIO/TA, BDT-1/TA, and BDT-2/TA is 6.32×10^{-4}, 7.21×10^{-4}, and 5.73×10^{-4} cm^2 V^{-1} s^{-1}, respectively; the corresponding μ_e/μ_h values are 0.75, 0.95, and 0.91, respectively. The μ_e values of the PBDB-T:TPT10 and PTQ10:TPT10-based devices are lower than those of the PM6:TPT10-based device, and the μ_e/μ_h value of the PM6:TPT10-based device is close to 1, which indicates balanced charge transport. Comparatively higher and more balanced μ_e and μ_h values are achieved in the blend with SAs, which are conducive to obtaining higher FF, reducing charge recombination, and improving the photovoltaic performance of the devices. The results indicate that a D/A bi-continuous network channel can be established to promote charge carrier transport in the blend film with a SA treatment.

To investigate the relationship between the blend morphology and photovoltaic performance of PSCs,[67] atomic force microscopy (AFM) images of the photovoltaic active layer were obtained, as shown in Fig. 5 and S5.† The surface roughness (R_q) of the PM6:TPT10 (1 : 1.2, w/w) blend with 0.25% DIO, 16 wt% BDT-1, and 16 wt% BDT-2 was 1.16, 1.00, and 0.96 nm, respectively. The PBDB-T:TPT10 blend film with 0.25% DIO additive showed an R_q value of 1.30 nm; the R_q value of the blends with 16 wt% BDT-1 and 16 wt% BDT-2 decreased to 0.98 nm and 0.87 nm, respectively. For the PTQ10:TPT10 system, blends with 0.25% DIO, 16 wt% BDT-1, and 16 wt% BDT-2 showed R_q values of 1.34, 1.20, and 0.84 nm, respectively. The blend films with SAs show a smaller R_q value than the films with the DIO additive, inducing better contact between the active layer and the interlayer which enhances the charge transport to obtain a higher FF. The phase morphology of PM6:TPT10, PBDB-T:TPT10 and PTQ10:TPT10 blends with 0.25% DIO, 16 wt% BDT-1, and 16 wt% BDT-2 were investigated by transmission electron microscopy (TEM) (Fig. S6†). As depicted in Fig. S6,† all the blends with SAs present uniform domain phases, being favorable for charge transport and thus resulting in high FF. However, with the additive of DIO, the domain morphology is observed to have increased aggregation, which decreases the interfaces between the donor and acceptor and limits the effective charge separation. Obviously, with the SAs of BDT-1 and BDT-2, the blends display a uniformly distributed nano-structured phase with a bicontinuous interpenetrating network, which is beneficial for exciton dissociation and charge transport, thus obtaining a high J_{SC} and FF.[68] SAs can improve the molecular arrangement and crystallinity, and the formation of appropriate crystallinity can not only reduce the surface roughness to adjust the favorable phase morphology, but also facilitate charge carrier transport and generate a high FF value. Moreover, the optimized surface morphology and uniform domains will enhance charge carrier transfer and charge collection and reduce charge recombination.[69]

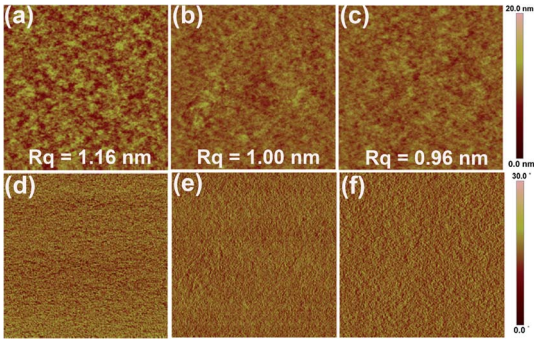

Fig. 5 AFM height (a–c) and phase (d–f) images of the PM6:TPT10 blend films (1 : 1.2, w/w) with the additive treatment of 0.25% DIO (a and d), 16 wt% BDT-1 (b and e) and 16 wt% BDT-2 (c and f), respectively.

To gain insight into the correlation of the critical role of SAs in the blend morphology of the devices,[32] grazing-incidence X-ray scattering (GIXS) was adopted to investigate the molecular packing and orientation of pure and blend films (Fig. 6, S7, and S8†); the corresponding GIXS parameters are outlined in Table S4.† The GIXS patterns of all the four pristine films showed lamellar (100) packing peaks in the in-plane (along q_{xy}) directions defined at q_{xy} = 0.26–0.29 $Å^{-1}$ and strong π–π stacking (010) peaks in the out-of-plane (along q_z) directions defined at q_z = 1.66–1.72 $Å^{-1}$, which indicates the preferential formation of face-on orientation, which is conducive to vertical charge transport. The d-spacing and crystalline coherence lengths (CCLs) of the out-of-plane (010) peaks and in-plane (100) were evaluated, as shown in Table S4.† The d-spacing (010) values for PM6, PBDT-T, PTQ10, and TPT10 were estimated to be 3.78, 3.75, 3.65, and 3.72 Å, respectively. The CCL (010) values for PM6, PBDT-T, PTQ10, and TPT10 were estimated to be 18.69,

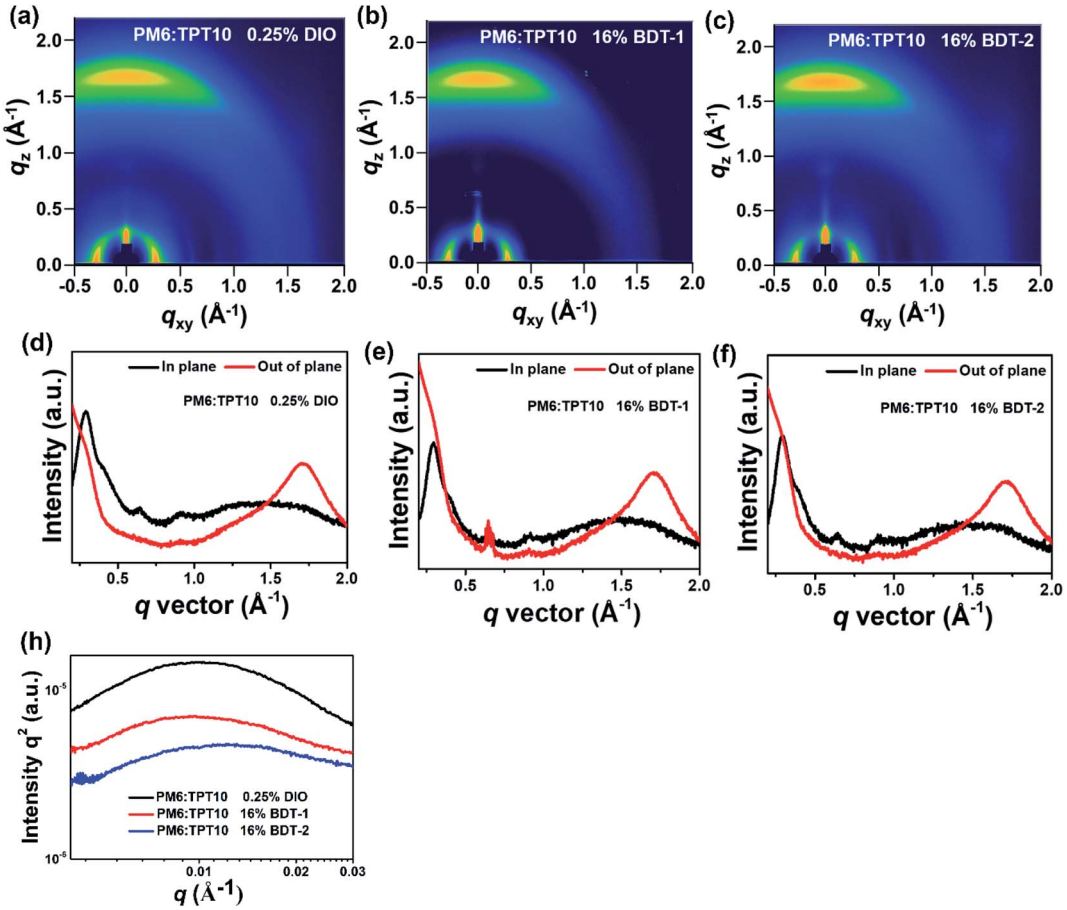

Fig. 6 2D GIXS patterns of PM6:TPT10 (1 : 1.2, w/w) blends with 0.25% DIO (a and d), 16 wt% BDT-1 (b and e), and 16 wt% BDT-2 (c and f) additives after thermal annealing, and the corresponding GIXS intensity profiles along the in-plane (black line) and out-of-plane (red line) directions; (h) R-SoXS profiles for PM6:TPT10 (1 : 1.2, w/w) blends with 0.25% DIO, 16 wt% BDT-1, and 16 wt% BDT-2 additives after thermal annealing.

22.36, 26.02, and 20.26 Å, respectively. The pure PTQ10 film shows the stronger intensity of the π–π stacking (010) peak. Clearly, in the lamellar (100) packing direction, the pure PM6 film showed the strongest peak with a CCL (100) of 46.557 Å, which implied better molecular arrangement. The PM6:TPT10 (1 : 1.2, w/w) blends with 0.25% DIO, 16 wt% BDT-1, and 16 wt% BDT-2 exhibited a π–π stacking CCL (010) of 23.51 Å (d = 3.70 Å), 24.08 Å (d = 3.70 Å), and 24.25 Å (d = 3.69 Å) in the out-of-plane direction, and a lamellar stacking CCL (100) of 70.00 Å (d = 21.87 Å), 82.83 Å (d = 21.51 Å), and 82.54 Å (d = 21.59 Å) in the in-plane direction, respectively. Likewise, the PBDB-T:TPT10 and PTQ10:TPT10 (1 : 1.2, w/w) blends showed a π–π stacking CCL (010) of 22.81 Å (d = 3.72 Å) and 25.62 Å (d = 3.64 Å) for 0.25% DIO, 23.62 Å (d = 3.70 Å) and 28.12 Å (d = 3.65 Å) for 16 wt% BDT-1, and 24.24 Å (d = 3.69 Å) and 27.89 Å (d = 3.64 Å) for 16 wt% BDT-2, respectively. Clearly, all the blends with SAs exhibit enhanced crystallinity and show a face-on orientation, which helps to increase charge transport.[70] In addition, the enhancement of crystallinity for blends can improve charge carrier transport, increase exciton dissociation, enhance the PSCs' stability performance, and reduce charge recombination.[69,71,72] These results suggest that an appropriate adjustment of molecular crystallinity is conducive to improving J_{SC} and FF values.[73]

To confirm that the favorable morphology with SAs is essential for improving the efficiency of the PSCs, resonant soft X-ray scattering (R-SoXS) with a photon energy of 284.2 eV was carried out to investigate the domain spacing and relative domain purity.[74–76] The q values of PM6:TPT10 (1 : 1.2, w/w) blends with 0.25% DIO, 16 wt% BDT-1, and 16 wt% BDT-2 were 0.099, 0.097, and 0.12 Å^{-1}, respectively (Fig. 6h and Table S5†), and their corresponding domain spacings were 63.5, 64.7, and 50.8 nm. Also, PTQ10:TPT10 (1 : 1.2, w/w) blends with 0.25% DIO, 16 wt% BDT-1, and 16 wt% BDT-2 had similar domain spacings of 51.8, 50.0, and 54.8 nm. Interestingly, the relative domain purities of PM6:TPT10 (1 : 1.2, w/w) blends with 0.25% DIO, 16 wt% BDT-1, and 16 wt% BDT-2 were estimated to 1, 0.82, and 0.70, respectively. Also, the PBDB-T:TPT10 and PTQ10:TPT10 blends had similar decreasing trends of domain purities by addition of 16 wt% BDT-1 and 16 wt% BDT-2. The relative domain purities of the PBDB-T:TPT10 and PTQ10:TPT10 blends were observed to be 0.90/0.93 for 0.25% DIO, 0.66/0.68 for 16 wt% BDT-1, and 0.73/0.74 for BDT-2, respectively (Fig. S9 and Table S5†). The decreased domain

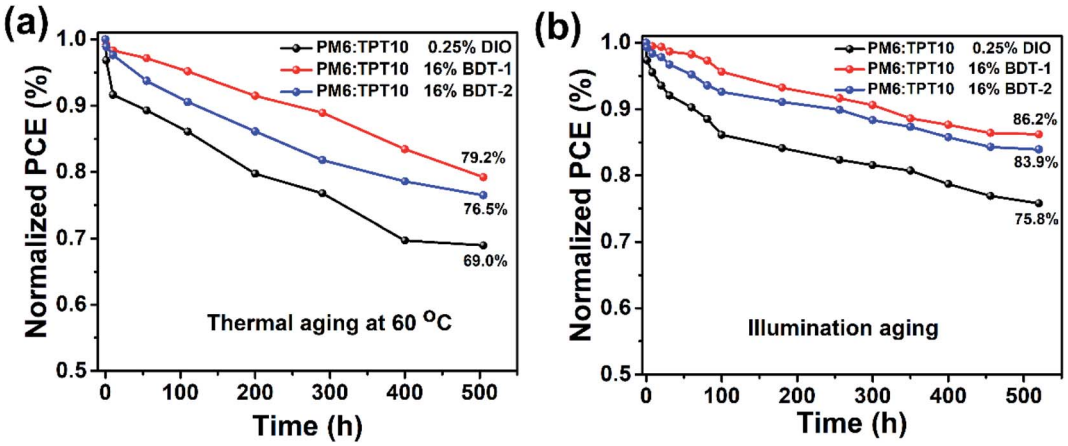

Fig. 7 Normalized PCEs of the PM6:TPT10 (1 : 1.2, w/w) based devices with 0.25% DIO, 16 wt% BDT-1, and 16 wt% BDT-2 additives at 60 °C with thermal aging time (a) and illumination aging time (under continuous 1 sun illumination) (b) in a nitrogen-filled glovebox.

purities of the blends by addition of BDT-1 and BDT-2 suggest the presence of more intermixed domains of the donor and acceptor, which is helpful for enhancing charge generation near the interface. Importantly, we observed that the V_{OC} value of the blend was slightly enhanced by addition of a BDT-1 SA. This could be attributed to the addition of the BDT-1 SA improving the morphological features and reducing energetic disorder near the interface, resulting in reduced energy loss and increased V_{OC}.[36,37,55,56]

It is a key strategy to modulate the morphology to meaningfully affect the thermal and photo-induced stability of devices for NF-PSCs.[77,78] Owing to the increased π–π packing CCL and intermolecular interaction in the blend with SAs compared to the device with a liquid additive, the effect of SAs is further assessed in the device stability. As shown in Fig. 7a, a quick "burn-in" photo-induced degradation, which only maintained 69.0% of the original PCE, was observed in the PM6:TPT10 (1 : 1.2, w/w)-based device with a 0.25% DIO additive under a constant temperature of 60 °C for 505 h in a nitrogen-filled glovebox. In comparison, identical devices with 16 wt% BDT-1 and 16 wt% BDT-2 maintained better PCE values, which decreased to 79.2% and 76.5% of their initial efficiency, respectively. However, the thermal stabilities of the PBDB-T:TPT10 and PTQ10:TPT10 devices are below that of the device based on PM6:TPT10 under the same conditions (Fig. S10†). The PCEs of PSCs with a SA treatment remain at a higher value compared to those with liquid additives in all devices. In addition to the thermal stability enhancement, the introduction of SAs also improved the photo-induced stability of the PSCs. As shown in Fig. 7b under continuous 1 sun illumination (provided by an array of white LEDs composed of the solar spectrum), the PCE of the device based on PM6:TPT10 (1 : 1.2, w/w) with 0.25% DIO was sharply attenuated to 75.8% (relative to its initial PCE value). The PM6:TPT10-based devices with 16 wt% BDT-1 and 16 wt% BDT-2 SAs still maintain 86.2% and 83.9% of their initial PCE after 520 h of sequential simulated solar radiation, respectively, whereas for other photovoltaic systems, the magnitude of attenuation is greater than that for the PM6:TPT10-based device (Fig. S10†). The results indicate that the SA treatment promotes morphological stability, which results in enhanced thermal and photo-induced stabilities of the photovoltaic devices due to the improved π–π packing CCLs and intermolecular interaction in the blend.

Conclusion

In summary, high-efficiency NF-PSCs were fabricated with two volatilizable and cost-effective quinone-based SAs, BDT-1 and BDT-2. The SA treatment increased the absorption intensity and redshifted the absorption spectra of the blend films. Compared to the DIO liquid additive treatment, the NF-PSC based on PM6:TPT10 (1 : 1.2, w/w) with the 16 wt% BDT-1 additive achieved the best PCE as high as 16.26% with a V_{OC} of 0.899 V, J_{SC} of 24.80 mA cm^{-2}, and FF of 73.00%. These values are superior to the PCE of 15.18% for the device with the 16 wt% BDT-2 additive and the PCE of 13.55% for the device with the 0.25% DIO additive. This is partly attributed to the favorable effect of suitable phase separated morphologies (*i.e.*, crystalline sizes and domain purities) between the donor and acceptor achieved by addition of SAs. Thus, the BDT-1 SA simultaneously improved the photovoltaic parameters V_{OC}, J_{SC}, and FF by enhancing light absorption, suppressing charge recombination, and improving charge collection. In addition, SAs contributed to the improvement of the thermal and photo-induced stabilities of the photovoltaic devices. These results indicate that SAs are promising processing additives for achieving higher-efficiency NF-PSCs in the future.

Conflicts of interest

The authors declare no competing financial interest.

Acknowledgements

This work was supported by the National Natural Science Foundation of China (No. 51763017 and 21602150), a National Research Foundation of Korea (NRF) grant funded by the Korea

government (MSIP) (2018R1A2A1A05077194), the Center for Advanced Soft-Electronics funded by the Ministry of Science and ICT as a Global Frontier Project (2012M3A6A5055225), the Wearable Platform Materials Technology Center (WMC; 2016R1A5A1009926) funded by the Korean Government (MSIT), and the Research Project Funded by Ulsan City (1.200042) and UK Brand (1.200030) of the UNIST (Ulsan National Institute of Science & Technology).

Notes and references

1 Y. Li, *Acc. Chem. Res.*, 2012, **45**, 723–733.
2 Y. Cui, H. Yao, J. Zhang, K. Xian, T. Zhang, L. Hong, Y. Wang, Y. Xu, K. Ma, C. An, C. He, Z. Wei, F. Gao and J. Hou, *Adv. Mater.*, 2020, 1908205.
3 N. Gasparini, A. Salleo, I. McCulloch and D. Baran, *Nat. Rev. Mater.*, 2019, **4**, 229–242.
4 J. Hou, O. Inganäs, R. H. Friend and F. Gao, *Nat. Mater.*, 2018, **17**, 119–128.
5 C. Lee, S. Lee, G.-U. Kim, W. Lee and B. J. Kim, *Chem. Rev.*, 2019, **119**, 8028–8086.
6 H. Fu, Z. Wang and Y. Sun, *Angew. Chem., Int. Ed.*, 2019, **58**, 4442–4453.
7 C. Cui and Y. Li, *Energy Environ. Sci.*, 2019, **12**, 3225–3246.
8 S. Dey, *Small*, 2019, **15**, 1900134.
9 D. Baran, N. Gasparini, A. Wadsworth, C. H. Tan, N. Wehbe, X. Song, Z. Hamid, W. Zhang, M. Neophytou, T. Kirchartz, C. J. Brabec, J. R. Durrant and I. McCulloch, *Nat. Commun.*, 2018, **9**, 2059.
10 T. Liu, Z. Luo, Y. Chen, T. Yang, Y. Xiao, G. Zhang, R. Ma, X. Lu, C. Zhan, M. Zhang, C. Yang, Y. Li, J. Yao and H. Yan, *Energy Environ. Sci.*, 2019, **12**, 2529–2536.
11 H. Chen, D. Hu, Q. Yang, J. Gao, J. Fu, K. Yang, H. He, S. Chen, Z. Kan, T. Duan, C. Yang, J. Ouyang, Z. Xiao, K. Sun and S. Lu, *Joule*, 2019, **3**, 3034–3047.
12 X. Xu, K. Feng, Y. W. Lee, H. Y. Woo, G. Zhang and Q. Peng, *Adv. Funct. Mater.*, 2020, **30**, 1907570.
13 Q. Fan, W. Su, S. Chen, W. Kim, X. Chen, B. Lee, T. Liu, U. A. Méndez-Romero, R. Ma, T. Yang, W. Zhuang, Y. Li, Y. Li, T.-S. Kim, L. Hou, C. Yang, H. Yan, D. Yu and E. Wang, *Joule*, 2020, **4**, 658–672.
14 Z. Luo, R. Sun, C. Zhong, T. Liu, G. Zhang, Y. Zou, X. Jiao, J. Min and C. Yang, *Sci. China: Chem.*, 2020, **63**, 361–369.
15 Y. Chang, T.-K. Lau, M.-A. Pan, X. Lu, H. Yan and C. Zhan, *Mater. Horiz.*, 2019, **6**, 2094–2102.
16 B. Jia, J. Wang, Y. Wu, M. Zhang, Y. Jiang, Z. Tang, T. P. Russell and X. Zhan, *J. Am. Chem. Soc.*, 2019, **141**, 19023–19031.
17 Z. Xing, X. Meng, R. Sun, T. Hu, Z. Huang, J. Min, X. Hu and Y. Chen, *Adv. Funct. Mater.*, 2020, 2000417.
18 Y. Zhang, Y. Wang, R. Ma, Z. Luo, T. Liu, S. Kang, H. Yan, Z. Yuan, C. Yang and Y. Chen, *Chinese J. Polym. Sci.*, 2020, DOI: 10.1007/s10118-020-2435-5.
19 T. Liu, R. Ma, Z. Luo, Y. Guo, G. Zhang, Y. Xiao, T. Yang, Y. Chen, G. Li, Y. Yi, X. Lu, H. Yan and B. Tang, *Energy Environ. Sci.*, 2020, DOI: 10.1039/D0EE00662A.
20 Z. Luo, R. Ma, T. Liu, J. Yu, Y. Xiao, R. Sun, G. Xie, J. Yuan, Y. Chen, K. Chen, G. Chai, H. Sun, J. Min, J. Zhang, Y. Zou, C. Yang, X. Lu, F. Gao and H. Yan, *Joule*, 2020, DOI: 10.1016/j.joule.2020.03.023.
21 T. Liu, Y. Zhang, Y. Shao, R. Ma, Z. Luo, Y. Xiao, T. Yang, X. Lu, Z. Yuan, H. Yan, Y. Chen and Y. Li, *Adv. Funct. Mater.*, 2020, 2000456.
22 S. Park, S. W. Heo, W. Lee, D. Inoue, Z. Jiang, K. Yu, H. Jinno, D. Hashizume, M. Sekino, T. Yokota, K. Fukuda, K. Tajima and T. Someya, *Nature*, 2018, **561**, 516–521.
23 S. Chen, S. Jung, H. J. Cho, N.-H. Kim, S. Jung, J. Xu, J. Oh, Y. Cho, H. Kim, B. Lee, Y. An, C. Zhang, M. Xiao, H. Ki, Z.-G. Zhang, J.-Y. Kim, Y. Li, H. Park and C. Yang, *Angew. Chem., Int. Ed.*, 2018, **57**, 13277–13282.
24 S. A. Hashemi, S. Ramakrishna and A. G. Aberle, *Energy Environ. Sci.*, 2020, **13**, 685–743.
25 T. Yan, W. Song, J. Huang, R. Peng, L. Huang and Z. Ge, *Adv. Mater.*, 2019, **31**, 1902210.
26 V. V. Brus, J. Lee, B. R. Luginbuhl, S.-J. Ko, G. C. Bazan and T.-Q. Nguyen, *Adv. Mater.*, 2019, **31**, 1900904.
27 R. Xia, C. J. Brabec, H.-L. Yip and Y. Cao, *Joule*, 2019, **3**, 2241–2254.
28 R. Sun, Q. Wu, J. Guo, T. Wang, Y. Wu, B. Qiu, Z. Luo, W. Yang, Z. Hu, J. Guo, M. Shi, C. Yang, F. Huang, Y. Li and J. Min, *Joule*, 2020, **4**, 407–419.
29 H. Yuk, B. Lu, S. Lin, K. Qu, J. Xu, J. Luo and X. Zhao, *Nat. Commun.*, 2020, **11**, 1604.
30 L. Liu, Y. Pei, S. Ma, X. Sun and T. J. Singler, *Adv. Eng. Mater.*, 2020, 1901351.
31 J. Yuan, Y. Zhang, L. Zhou, G. Zhang, H.-L. Yip, T.-K. Lau, X. Lu, C. Zhu, H. Peng, P. A. Johnson, M. Leclerc, Y. Cao, J. Ulanski, Y. Li and Y. Zou, *Joule*, 2019, **3**, 1140–1151.
32 L. Liu, Y. Kan, K. Gao, J. Wang, M. Zhao, H. Chen, C. Zhao, T. Jiu, A.-K.-Y. Jen and Y. Li, *Adv. Mater.*, 2020, **32**, 1907604.
33 H. Sun, T. Liu, J. Yu, T.-K. Lau, G. Zhang, Y. Zhang, M. Su, Y. Tang, R. Ma, B. Liu, J. Liang, K. Feng, X. Lu, X. Guo, F. Gao and H. Yan, *Energy Environ. Sci.*, 2019, **12**, 3328–3337.
34 D. Mo, H. Chen, J. Zhou, N. Tang, L. Han, Y. Zhu, P. Chao, H. Lai, Z. Xie and F. He, *J. Mater. Chem. A*, 2020, **8**, 8903–8912.
35 L. Hong, H. Yao, Z. Wu, Y. Cui, T. Zhang, Y. Xu, R. Yu, Q. Liao, B. Gao, K. Xian, H. Y. Woo, Z. Ge and J. Hou, *Adv. Mater.*, 2019, **31**, 1903441.
36 B. Fan, D. Zhang, M. Li, W. Zhong, Z. Zeng, L. Ying, F. Huang and Y. Cao, *Sci. China: Chem.*, 2019, **62**, 746–752.
37 Q. Yang, S. Yu, P. Fu, W. Yu, Y. Liu, X. Liu, Z. Feng, X. Guo and C. Li, *Adv. Funct. Mater.*, 2020, 1910205.
38 C. Sun, S. Qin, R. Wang, S. Chen, F. Pan, B. Qiu, Z. Shang, L. Meng, C. Zhang, M. Xiao, C. Yang and Y. Li, *J. Am. Chem. Soc.*, 2020, **142**, 1465–1474.
39 L. Zhu, M. Zhang, G. Zhou, T. Hao, J. Xu, J. Wang, C. Qiu, N. Prine, J. Ali, W. Feng, X. Gu, Z. Ma, Z. Tang, H. Zhu, L. Ying, Y. Zhang and F. Liu, *Adv. Energy Mater.*, 2020, 1904234.
40 J. Fu, S. Chen, K. Yang, S. Jung, J. Lv, L. Lan, H. Chen, D. Hu, Q. Yang, T. Duan, Z. Kan, C. Yang, K. Sun, S. Lu, Z. Xiao and Y. Li, *iScience*, 2020, **23**, 100965.

41 J. Cai, H. Wang, X. Zhang, W. Li, D. Li, Y. Mao, B. Du, M. Chen, Y. Zhuang, D. Liu, H.-L. Qin, Y. Zhao, J. A. Smith, R. C. Kilbride, A. J. Parnell, R. A. L. Jones, D. G. Lidzey and T. Wang, *J. Mater. Chem. A*, 2020, **8**, 4230–4238.
42 S. Liu, J. Yuan, W. Deng, M. Luo, Y. Xie, Q. Liang, Y. Zou, Z. He, H. Wu and Y. Cao, *Nat. Photonics*, 2020, **14**, 300–305.
43 R. Ma, T. Liu, Z. Luo, Q. Guo, Y. Xiao, Y. Chen, X. Li, S. Luo, X. Lu, M. Zhang, Y. Li and H. Yan, *Sci. China: Chem.*, 2020, **63**, 325–330.
44 L. Zhan, S. Li, T.-K. Lau, Y. Cui, X. Lu, M. Shi, C.-Z. Li, H. Li, J. Hou and H. Chen, *Energy Environ. Sci.*, 2020, **13**, 635–645.
45 Y. Cui, H. Yao, L. Hong, T. Zhang, Y. Tang, B. Lin, K. Xian, B. Gao, C. An, P. Bi, W. Ma and J. Hou, *Natl. Sci. Rev.*, 2020, DOI: 10.1093/nsr/nwz200.
46 C. Sun, F. Pan, H. Bin, J. Zhang, L. Xue, B. Qiu, Z. Wei, Z.-G. Zhang and Y. Li, *Nat. Commun.*, 2018, **9**, 743.
47 Y. Zhu, A. Gadisa, Z. Peng, M. Ghasemi, L. Ye, Z. Xu, S. Zhao and H. Ade, *Adv. Energy Mater.*, 2019, **9**, 1900376.
48 Y. Lin, Y. Jin, S. Dong, W. Zheng, J. Yang, A. Liu, F. Liu, Y. Jiang, T. P. Russell, F. Zhang, F. Huang and L. Hou, *Adv. Energy Mater.*, 2018, **8**, 1701942.
49 L. Ye, W. Zhao, S. Li, S. Mukherjee, J. H. Carpenter, O. Awartani, X. Jiao, J. Hou and H. Ade, *Adv. Energy Mater.*, 2017, **7**, 1602000.
50 H. B. Naveed, K. Zhou and W. Ma, *Acc. Chem. Res.*, 2019, **52**, 2904–2915.
51 S. Zhang, L. Ye, W. Zhao, B. Yang, Q. Wang and J. Hou, *Sci. China: Chem.*, 2015, **58**, 248–256.
52 W. Köntges, P. Perkhun, J. Kammerer, R. Alkarsifi, U. Würfel, O. Margeat, C. Videlot-Ackermann, J.-J. Simon, R. R. Schröder, J. Ackermann and M. Pfannmöller, *Energy Environ. Sci.*, 2020, **13**, 1259–1268.
53 A. J. Moulé and K. Meerholz, *Adv. Mater.*, 2008, **20**, 240–245.
54 Y. Zhang, X. Guo, B. Guo, W. Su, M. Zhang and Y. Li, *Adv. Funct. Mater.*, 2017, **27**, 1603892.
55 J. Zhao, Y. Li, G. Yang, K. Jiang, H. Lin, H. Ade, W. Ma and H. Yan, *Nat. Energy*, 2016, **1**, 15027.
56 Y. Zhou, K. L. Gu, X. Gu, T. Kurosawa, H. Yan, Y. Guo, G. I. Koleilat, D. Zhao, M. F. Toney and Z. Bao, *Chem. Mater.*, 2016, **28**, 5037–5042.
57 H. Yan, Y. Tang, X. Sui, Y. Liu, B. Gao, X. Liu, S. F. Liu, J. Hou and W. Ma, *ACS Energy Lett.*, 2019, **4**, 1356–1363.
58 B. J. Tremolet de Villers, K. A. O'Hara, D. P. Ostrowski, P. H. Biddle, S. E. Shaheen, M. L. Chabinyc, D. C. Olson and N. Kopidakis, *Chem. Mater.*, 2016, **28**, 876–884.
59 R. Yu, H. Yao, Z. Chen, J. Xin, L. Hong, Y. Xu, Y. Zu, W. Ma and J. Hou, *Adv. Mater.*, 2019, **31**, 1900477.
60 R. Yu, H. Yao, L. Hong, Y. Qin, J. Zhu, Y. Cui, S. Li and J. Hou, *Nat. Commun.*, 2018, **9**, 4645.
61 M. Zhang, X. Guo, W. Ma, H. Ade and J. Hou, *Adv. Mater.*, 2015, **27**, 4655–4660.
62 S. Li, L. Ye, W. Zhao, S. Zhang, S. Mukherjee, H. Ade and J. Hou, *Adv. Mater.*, 2016, **28**, 9423–9429.
63 Y. Zhang, L. Shi, T. Yang, T. Liu, Y. Xiao, X. Lu, H. Yan, Z. Yuan, Y. Chen and Y. Li, *J. Mater. Chem. A*, 2019, **7**, 26351–26357.
64 Y. Chen, P. Ye, Z.-G. Zhu, X. Wang, L. Yang, X. Xu, X. Wu, T. Dong, H. Zhang, J. Hou, F. Liu and H. Huang, *Adv. Mater.*, 2017, **29**, 1603154.
65 A. K. K. Kyaw, D. H. Wang, V. Gupta, W. L. Leong, L. Ke, G. C. Bazan and A. J. Heeger, *ACS Nano*, 2013, **7**, 4569–4577.
66 G. Feng, J. Li, Y. He, W. Zheng, J. Wang, C. Li, Z. Tang, A. Osvet, N. Li, C. J. Brabec, Y. Yi, H. Yan and W. Li, *Joule*, 2019, **3**, 1765–1781.
67 Y. Zhang, Y. Wang, T. Yang, T. Liu, Y. Xiao, X. Lu, H. Yan, Z. Yuan, Y. Chen and Y. Li, *ACS Appl. Mater. Interfaces*, 2019, **11**, 32218–32224.
68 Y. Ding, X. Zhang, H. Feng, X. Ke, L. Meng, Y. Sun, Z. Guo, Y. Cai, C. Jiao, X. Wan, C. Li, N. Zheng, Z. Xie and Y. Chen, *ACS Appl. Mater. Interfaces*, 2020, DOI: 10.1021/acsami.acsami.0c05331.
69 C. Huang, H. Yu, J. Chen, J. Zhang, Z. Wu and C. Hou, *Sol. Energy Mater. Sol. Cells*, 2019, **200**, 110030.
70 C. Lee, T. Giridhar, J. Choi, S. Kim, Y. Kim, T. Kim, W. Lee, H.-H. Cho, C. Wang, H. Ade and B. J. Kim, *Chem. Mater.*, 2017, **29**, 9407–9415.
71 Z. Wu, H. Yu, S. Shi and Y. Li, *J. Mater. Chem. A*, 2019, **7**, 14776–14789.
72 C. Huang and H. Yu, *ACS Appl. Mater. Interfaces*, 2020, **12**, 19643–19654.
73 T. Liu, Z. Luo, Q. Fan, G. Zhang, L. Zhang, W. Gao, X. Guo, W. Ma, M. Zhang, C. Yang, Y. Li and H. Yan, *Energy Environ. Sci.*, 2018, **11**, 3275–3282.
74 H.-H. Cho, S. Kim, T. Kim, V. G. Sree, S.-H. Jin, F. S. Kim and B. J. Kim, *Adv. Energy Mater.*, 2018, **8**, 1701436.
75 C. Lee, Y. Li, W. Lee, Y. Lee, J. Choi, T. Kim, C. Wang, E. D. Gomez, H. Y. Woo and B. J. Kim, *Macromolecules*, 2016, **49**, 5051–5058.
76 X. Jiao, L. Ye and H. Ade, *Adv. Energy Mater.*, 2017, **7**, 1700084.
77 W. Yang, Z. Luo, R. Sun, J. Guo, T. Wang, Y. Wu, W. Wang, J. Guo, Q. Wu, M. Shi, H. Li, C. Yang and J. Min, *Nat. Commun.*, 2020, **11**, 1218.
78 Y. Dong, Y. Zou, J. Yuan, H. Yang, Y. Wu, C. Cui and Y. Li, *Adv. Mater.*, 2019, **31**, 1904601.

